AFRL-OSR-VA-TR-2013-0134

Measurements in Regions of Shock Wave/Turbulent Boundary Layer Interaction from Mach 3 to 10 for Open and "Blind" Code Evaluation/Validation

Michael S. Holden, Timothy P. Wadhams, Matthew G. MacLean, Aaron Dufrene

CUBRC, Inc

March 2013
Final Report

AIR FORCE RESEARCH LABORATORY
AF OFFICE OF SCIENTIFIC RESEARCH (AFOSR)
ARLINGTON, VIRGINIA 22203
AIR FORCE MATERIEL COMMAND

REPORT DOCUMENTATION PAGE

Form Approved
OMB No. 0704-0188

PLEASE DO NOT RETURN YOUR FORM TO THE ABOVE ORGANIZATION.

1. REPORT DATE *(DD-MM-YYYY)*	2. REPORT TYPE	3. DATES COVERED *(From - To)*
10-01-2013		Sep 2011 - Sep 2012

4. TITLE AND SUBTITLE

Measurements in Regions of Shock Wave/Turbulent Boundary Layer Interaction from Mach 3 to 10 for Open and "Blind" Code Evaluation/Validation

5a. CONTRACT NUMBER

5b. GRANT NUMBER

FA9550-11-1-0290

5c. PROGRAM ELEMENT NUMBER

6. AUTHOR(S)

Holden, Michael S.
Wadhams, Timothy P.
MacLean, Matthew G.
DuFrene, Aaron

5d. PROJECT NUMBER

5e. TASK NUMBER

5f. WORK UNIT NUMBER

7. PERFORMING ORGANIZATION NAME(S) AND ADDRESS(ES)

CUBRC, Inc.
4455 Genesee Street, Suite 106
Buffalo, NY 14225

8. PERFORMING ORGANIZATION REPORT NUMBER

9. SPONSORING/MONITORING AGENCY NAME(S) AND ADDRESS(ES)

USAF, AFRL, AF Office of Scientific Research
875 N. RAndolph Street, Room 3112
Arlington, VA 22203

10. SPONSOR/MONITOR'S ACRONYM(S)

11. SPONSOR/MONITOR'S REPORT NUMBER(S)

AFRL-OSR-VA-TR-2013-0134

12. DISTRIBUTION/AVAILABILITY STATEMENT

DISTRIBUTION A: APPROVED FOR PUBLIC RELEASE

13. SUPPLEMENTARY NOTES

14. ABSTRACT

Experimental studies have been conducted to examine the characteristics of regions of shock wave/turbulent boundary layer interaction over cone/flare and hollow cylinder/flare configurations in high Reynolds number flows at Mach numbers between 5 and 10 in cold flows and in flows with duplicated flight velocities. Detailed surface pressure and heat transfer measurements have been made through the separated interaction regions as well as upstream and downstream of the interactions for a range of Reynolds numbers under cold wall conditions for total enthalpies duplicating flight The large scale of the models used in these experiments enabled us to obtain measurements in fully turbulent flows with the length of turbulent flow up to 1,000 boundary layer thicknesses downstream of the beginning of untripped transition. The surface measurements obtained in these studies together with Schlieren and interferometry measurements of the regions of shock wave/boundary layer interaction have been assembled to provide data sets for “blind” code validation studies.

15. SUBJECT TERMS

shock wave/turbulent boundary layer interaction;

16. SECURITY CLASSIFICATION OF:			17. LIMITATION OF ABSTRACT	18. NUMBER OF PAGES	19a. NAME OF RESPONSIBLE PERSON
a. REPORT	b. ABSTRACT	c. THIS PAGE			Timothy P Wadhams
U	U	U	U		19b. TELEPHONE NUMBER *(Include area code)* 716.204.5125

Reset

INSTRUCTIONS FOR COMPLETING SF 298

1. REPORT DATE. Full publication date, including day, month, if available. Must cite at least the year and be Year 2000 compliant, e.g. 30-06-1998; xx-06-1998; xx-xx-1998.

2. REPORT TYPE. State the type of report, such as final, technical, interim, memorandum, master's thesis, progress, quarterly, research, special, group study, etc.

3. DATES COVERED. Indicate the time during which the work was performed and the report was written, e.g., Jun 1997 - Jun 1998; 1-10 Jun 1996; May - Nov 1998; Nov 1998.

4. TITLE. Enter title and subtitle with volume number and part number, if applicable. On classified documents, enter the title classification in parentheses.

5a. CONTRACT NUMBER. Enter all contract numbers as they appear in the report, e.g. F33615-86-C-5169.

5b. GRANT NUMBER. Enter all grant numbers as they appear in the report, e.g. AFOSR-82-1234.

5c. PROGRAM ELEMENT NUMBER. Enter all program element numbers as they appear in the report, e.g. 61101A.

5d. PROJECT NUMBER. Enter all project numbers as they appear in the report, e.g. 1F665702D1257; ILIR.

5e. TASK NUMBER. Enter all task numbers as they appear in the report, e.g. 05; RF0330201; T4112.

5f. WORK UNIT NUMBER. Enter all work unit numbers as they appear in the report, e.g. 001; AFAPL30480105.

6. AUTHOR(S). Enter name(s) of person(s) responsible for writing the report, performing the research, or credited with the content of the report. The form of entry is the last name, first name, middle initial, and additional qualifiers separated by commas, e.g. Smith, Richard, J, Jr.

7. PERFORMING ORGANIZATION NAME(S) AND ADDRESS(ES). Self-explanatory.

8. PERFORMING ORGANIZATION REPORT NUMBER. Enter all unique alphanumeric report numbers assigned by the performing organization, e.g. BRL-1234; AFWL-TR-85-4017-Vol-21-PT-2.

9. SPONSORING/MONITORING AGENCY NAME(S) AND ADDRESS(ES). Enter the name and address of the organization(s) financially responsible for and monitoring the work.

10. SPONSOR/MONITOR'S ACRONYM(S). Enter, if available, e.g. BRL, ARDEC, NADC.

11. SPONSOR/MONITOR'S REPORT NUMBER(S). Enter report number as assigned by the sponsoring/ monitoring agency, if available, e.g. BRL-TR-829; -215.

12. DISTRIBUTION/AVAILABILITY STATEMENT. Use agency-mandated availability statements to indicate the public availability or distribution limitations of the report. If additional limitations/ restrictions or special markings are indicated, follow agency authorization procedures, e.g. RD/FRD, PROPIN, ITAR, etc. Include copyright information.

13. SUPPLEMENTARY NOTES. Enter information not included elsewhere such as: prepared in cooperation with; translation of; report supersedes; old edition number, etc.

14. ABSTRACT. A brief (approximately 200 words) factual summary of the most significant information.

15. SUBJECT TERMS. Key words or phrases identifying major concepts in the report.

16. SECURITY CLASSIFICATION. Enter security classification in accordance with security classification regulations, e.g. U, C, S, etc. If this form contains classified information, stamp classification level on the top and bottom of this page.

17. LIMITATION OF ABSTRACT. This block must be completed to assign a distribution limitation to the abstract. Enter UU (Unclassified Unlimited) or SAR (Same as Report). An entry in this block is necessary if the abstract is to be limited.

MEASUREMENTS IN REGIONS OF SHOCK WAVE/TURBULENT BOUNDARY LAYER INTERACTION FROM MACH 4 TO 10 FOR OPEN AND "BLIND" CODE EVALUATION/VALIDATION

ABSTRACT

Experimental studies have been conducted to examine the characteristics of regions of shock wave/turbulent boundary layer interaction over cone/flare and hollow cylinder/flare configurations in high Reynolds number flows at Mach numbers between 5 and 10 in cold flows and in flows with duplicated flight velocities. Detailed surface pressure and heat transfer measurements have been made through the separated interaction regions as well as upstream and downstream of the interactions for a range of Reynolds numbers under cold wall conditions for total enthalpies duplicating flight The large scale of the models used in these experiments enabled us to obtain measurements in fully turbulent flows with the length of turbulent flow up to 1,000 boundary layer thicknesses downstream of the beginning of untripped transition. The surface measurements obtained in these studies together with Schlieren and interferometry measurements of the regions of shock wave/boundary layer interaction have been assembled to provide data sets for "blind" code validation studies. We have also included detailed information on the results of experimental studies of shock wave/boundary layer interaction conducted earlier which can also be used to evaluate the models of turbulence employed in CFD codes.

INTRODUCTION

The accurate prediction of the scale and aerothermal loads generated in separated regions of shock wave/turbulent boundary layer interaction remains one of the most formidable computational tasks, principally because of the difficulty in modeling the nonequilibrium turbulence and shock interaction flow phenomena in the separation and reattachment regions. To predict these flows with RANS techniques, the nonequilibrium nature of the turbulent processes in the separation and reattachment regions requires models that are significantly more sophisticated than those required to describe attached flows in mild pressure gradients. When more sophisticated numerical techniques are employed to describe these flows, such as LES, again the "Achilles heel" is the modeling of the wall layer and the unsteady shock- turbulence interaction phenomena, which are key to describing the mechanisms of flow separation and reattachment. In order to advance the development of both RANS and LES methods, it is of major importance to provide detailed measurements in fully turbulent separated regions over well-defined configurations in both "true temperature" and "cold" supersonic and hypersonic flows with boundary and flow conditions to provide the basis for selecting and evaluating the models of turbulence. Currently there are virtually no measurements under cold-wall conditions where the total enthalpy of the flow matches the flight Mach number that are required to resolve key questions associated with compressibility and real gas effects on the size and structure of separated turbulent interaction regions. The experiments conducted in the current studies which were made at total enthalpies which corresponded to flight velocity at the test Mach number between 5 and 9 were designed to remedy this situation.

Most of the experiments conducted over the past 50 years to provide data on both wedge- and shock-induced turbulent separated regions in supersonic and hypersonic flows suffer from deficiencies associated with the transitional nature of the flow upstream of the interaction and well-defined boundary conditions associated with the experimental configuration or extraneous disturbances introduced into the tunnel wall boundary layer upstream of the interaction. There continues to be a debate as to whether the gross unsteady nature of the separated region observed in many experiments results from transition or tripping on models supported in the tunnel or from upstream effects on the tunnel walls. While many experiments with separated interaction regions have been conducted with two-dimensional configurations, the lack of well-defined boundary conditions has always provided a major stumbling block to the numerical simulation of these flows. This is true even with the large flat-plate wedge- and flat-plate shock-generated configurations that have been employed to study laminar and turbulent shock boundary layer interaction over a large range of test conditions at CUBRC. In this experimental program we have employed axisymmetric

**Fellow, AIAA, Vice President-Hypersonics, CUBRC, 4455 Genesee Street, Buffalo, NY 14225*

*** Member, AIAA, Project Engineers, CUBRC, 4455 Genesee Street, Buffalo, NY 14225*

This work was supported by AFOSR Grant No. FA9550-11-1-0290

configurations such as hollow cylinder/flare and double cone models to provide measurements on configurations with well-defined boundary conditions. In these experiments, the regions of boundary layer transition are well defined and are well upstream of the interaction regions. Also, the conditions in the freestream are verified both by surveys and computations from the reservoir conditions.

The major objective of the current program is to provide detailed surface measurements in regions of shock wave/**turbulent** boundary layer interaction to produce datasets, for "blind" code validation activity similar to that we conducted earlier for laminar flows. We have also selected from our earlier studies a number of test cases for which we have presented the full datasets to provide "open " measurements of the distributions of heat transfer and pressure for the initial evaluation of the codes.

REVIEW OF RECENT COMPARISONS BETWEEN PREDICTIONS AND EXPERIMENTS IN HYPERSONIC TURBULENT INTERACTIONS (OPEN TEST CASES)

Our recent experimental programs have employed large axisymmetric models to provide separated regions of shock wave/turbulent boundary layer interactions with well-defined model and flow boundary conditions, and we have performed the testing at high Reynolds numbers to place boundary layer transition at least 100 boundary layer thicknesses ahead of the shock interaction region. The large cone/flare model shown in Figure 1(a) was constructed not only to generate high Reynolds number in the interaction region but also to provide large boundary layer thicknesses which could be surveyed with probes which could resolve details of the wall region of the turbulent boundary layer. Although the full-scale HIFiRE 1 model shown in Figure 1(b) was restricted in size because of the dimensional requirements associated with the launch system, measurements were obtained with well-defined turbulent boundary layers and, for the cases we have selected for code validation, we achieved transition well upstream on the fore-cone without boundary layer trips. The length of the flare again was selected based on launch vehicle requirements and as shown later was just sufficient to provide a good downstream boundary condition.

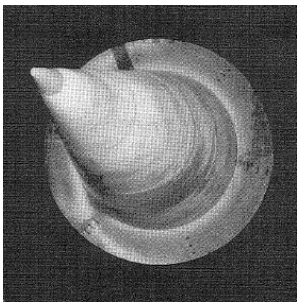

(a) Large Cone/Flare Model

(b) HIFiRE 1 Model

Figure 1 Cone Flare and Cone Cylinder Flare Models to Examine Turbulent Separated Flows over Cone Flare Junctions

Although we obtained measurements on the large cone/flare model, in an experimental program before we tested the HIFiRE 1 configuration, at that time we did not have the resources to compare data with RANS calculations incorporating contemporary turbulence modeling as was done during and after our tests with the HIFiRE configuration. The initial flare configuration for HIFiRE 1 was a 36° flare and it was clear from our initial tests duplicating flight conditions that, although pretest predictions indicated a small separated region, our measurements indicated an extensive separated flow spreading from the downstream edge of the flare over the cylindrical section of the model was developed which would not provide a satisfactory code validation dataset. Based on subsequent measurements, we selected a configuration with a 33° flare to provide a well-defined separated flow at the cylinder/flare junction with sufficient distance downstream to provide well-defined downstream conditions. For the conditions at which these experiments were conducted, code predictions of the flow upstream and in the interaction region were obtained with the Shear Stress Transport (SST)[1] Model and the Spalart-Allmaras (SA) Model. Predictions of the turbulent flow upstream of the interaction regions (as shown in Figure 2) surprisingly gave very different results and clearly issues associated with the discrepancies between theory and experiment should be solved before

embarking on comparisons in the interaction region. This discrepancy between theory and measurement for the turbulent heating levels over a cone was observed earlier in experiments performed at Mach 10 flight conditions. Shown in Figure 3, while the heat transfer measurements in laminar flow were in excellent agreement with prediction, measured turbulent heating was significantly less than predicted with the SA, SST and Baldwin-Lomax turbulence models. The calculations of the size of the separated interaction region (shown in Figure 4) demonstrate that the SST model significantly overpredicts the size of the separated region, while the SA model predicting an attached flow in the corner.

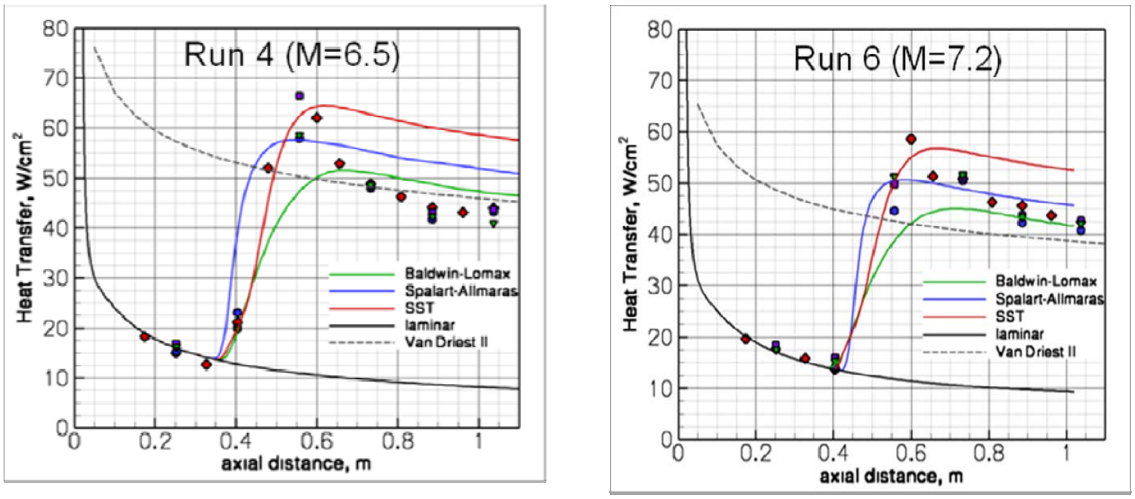

Figure 2 Comparisons between Measurements Upstream of the Interaction Region and Predictions for a Range of Turbulence Models

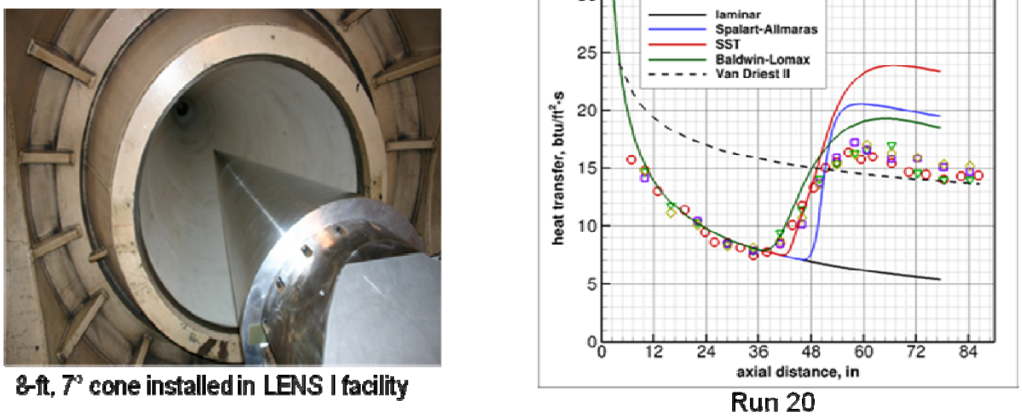

Figure 3 Comparisons between Measurement Sets of Heat Transfer at Mach 10 Flight Conditions and RANS Prediction Methods

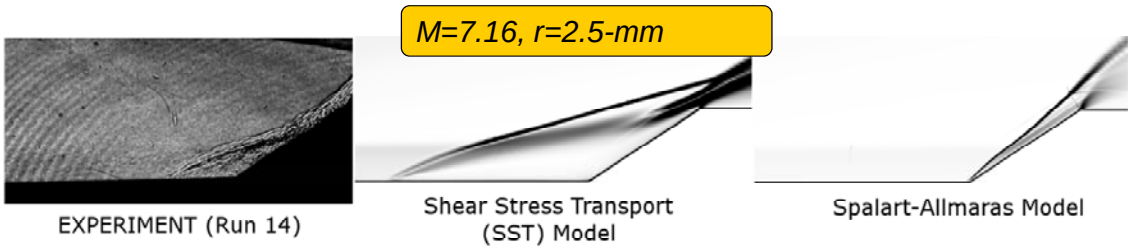

Figure 4 Comparison between Measured Size of Separated Region on HIFiRE 1 Model and Original Predictions with DPLR using SST and SA Turbulence Models

An empirical modification to these methods suggested by Wilcox[2] was employed to limit the generation of shear stress by introducing an empirical coefficient C_{LIM} in the shear stress production equation. Figure 5 shows the results of employing different values for this coefficient. For this set of experimental conditions, a value of C_{LIM} = 0.9 provides the most accurate method of predicting the separated flow. For this value RANS calculations are in reasonable agreement with the pressure and heat transfer measurements obtained in the interaction regions over the cylinder/flare as shown in this figure.

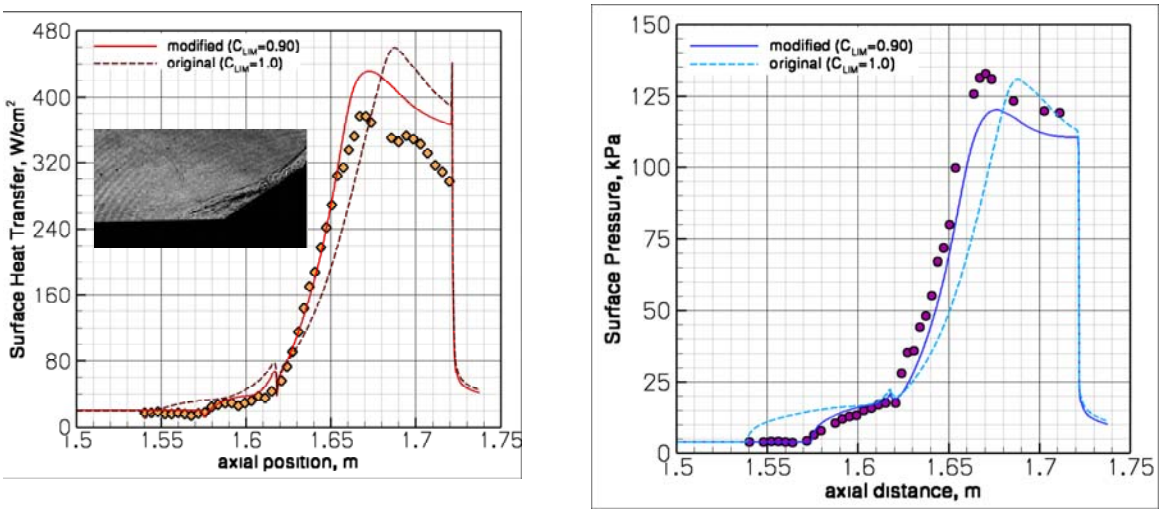

Figure 5 Comparison between DPLR/RANS Solutions and Heat Transfer and Pressure Measurements at the Cylinder Flare Junction on the HIFiRE 1 Configuration

Comparisons between Computations and Measurements obtained Earlier in Separated Flow over Flat Plate/Wedge and Flat Plate/ Shock Generator Models

Earlier extensive sets of measurements were made with flat plate/wedge and flat plate/shock generator configurations at CUBRC over the past 30 years. We have selected two test cases from this dataset which we believe present the most useful from the viewpoint of code validation. Two of the models used in these studies are shown in Figure 6.

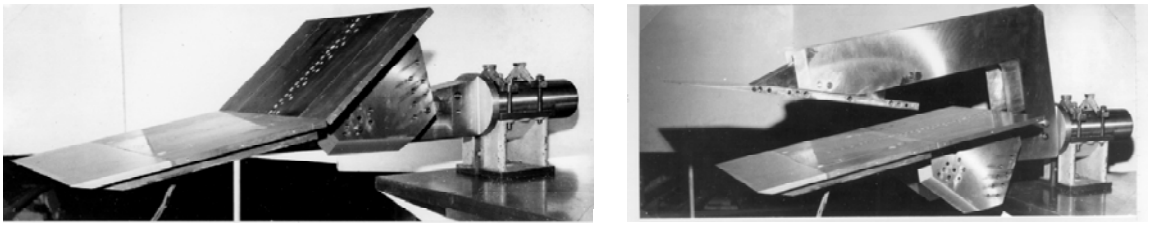

(a) Wedge Interaction Model **(b) Shock Interaction Model**

Figure 6 Two-dimensional Models to Examine Shock Wave/Turbulent Boundary Layer Interaction in Compression Corners and Externally Developed Shocks Incident on the Turbulent Boundary Layer

Regions of flow separation either induced at compression corners or by incident shocks in hypersonic flows are complex in nature, principally because flow separation takes place initially at the base of the turbulent boundary layer and the recirculation region is often embedded in the incoming boundary layer as

illustrated in the sequence of photographs for wedge- and shock-induced separated regions shown in Figure 7. Of significant interest here is that the wedge-shock extends into the sublayer of the turbulent flows, initially creating a tiny embedded recirculating region at the flat plate wedge junction or at the base of the incident shock. In both cases, separation shock traverses and interacts with the turbulence in the incoming boundary layer. Only when turning angles of over 36° are imposed on the flow are well-separated flows generated which extend the full width of the boundary layer. Modeling the turbulence generated through the interaction region of these flows is clearly a formidable task and selecting the models which most accurately represent these phenomena will require detailed flowfield as well as surface measurements.

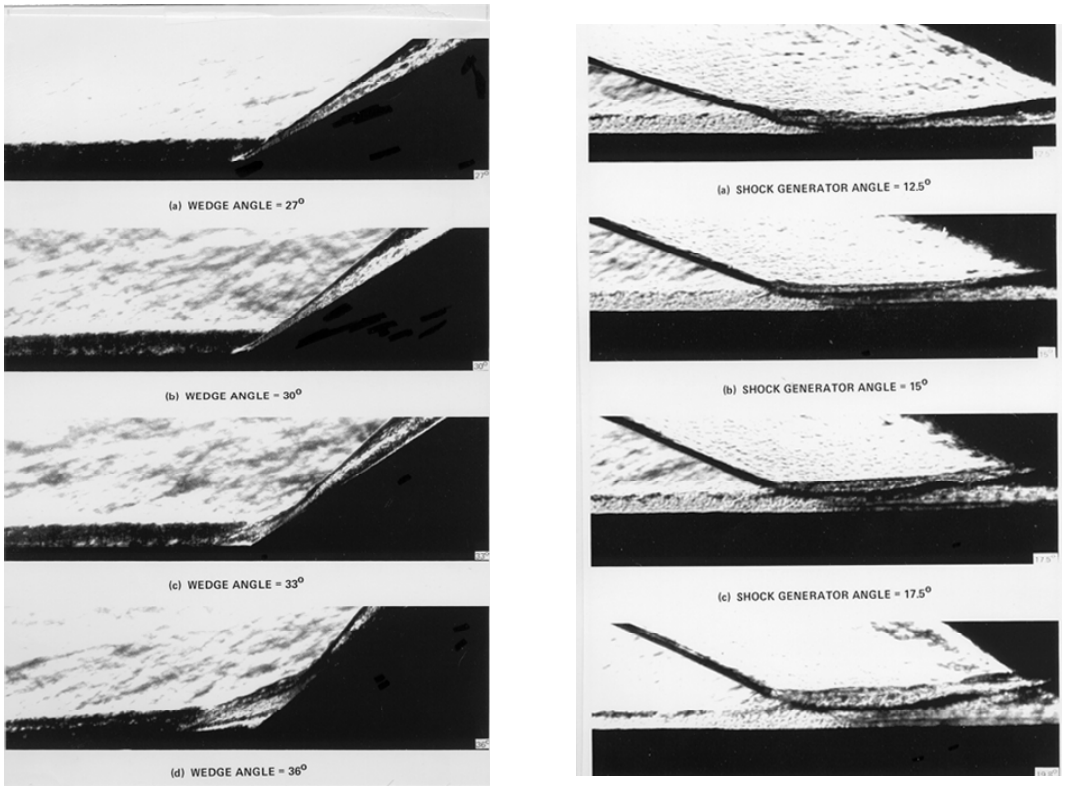

Figure 7 Schlieren Photographs of Turbulent Separated Flows at Wedge Compression Corners and Induced by Incident Shock/Turbulent Boundary Layer Interaction

When we employed the DPLR method with a turbulence model which best fit the measurements over the HIFiRE configuration to describe flow for these two configurations, we significantly overpredicted the size of the interaction region. Figure 8 shows the comparisons for the flat plate/36° wedge configuration, and Figure 9 show similar comparisons for the separated flows introduced by incident shock. In both cases, the computations capture with good accuracy the pressure and heating levels both upstream and downstream of the separated interaction regions. Clearly, the turbulence models employed here are totally inadequate in describing the length and properties of the interaction regions whether the pressure rise is induced internally as in the case of the compression corner or externally by an incident shock. It should be noted here that computations for the incident shock cases are made significantly more complicated because of the requirement to compute the flow over the shock generator including the position of transition all of which can influence the position of the incident shock. This added complexity has coupled with those associated with lateral boundary conditions make the axisymmetric cone/flare and hollow cylinder flare models far more suitable for code validation

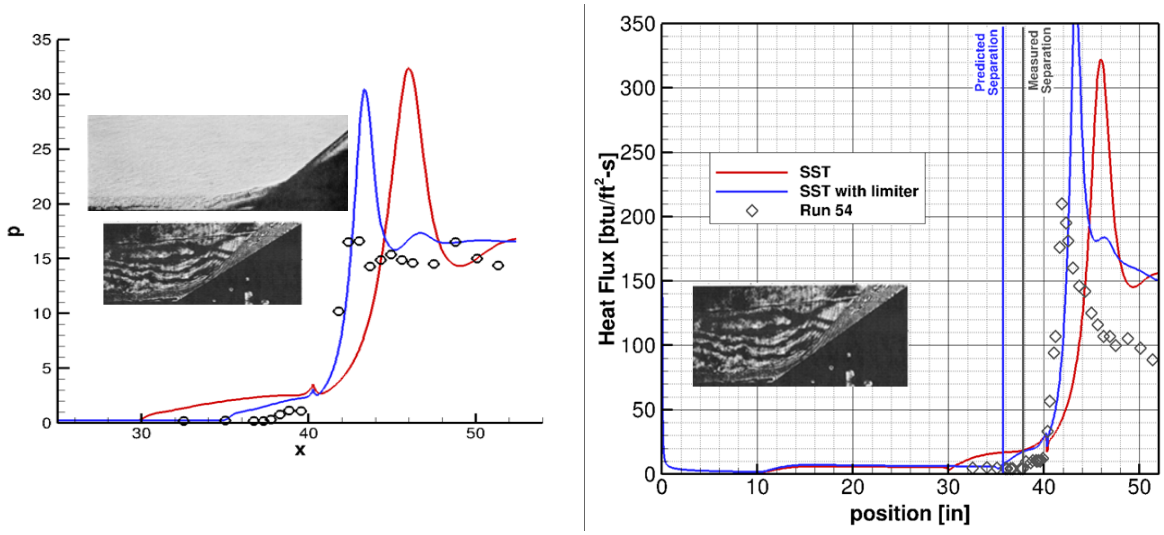

Figure 8 **Comparisons between DPLR/RANS Predictions and Measurements of Pressure and Heat Transfer in Separated Flows over a Flat Plate Wedge Configuration**

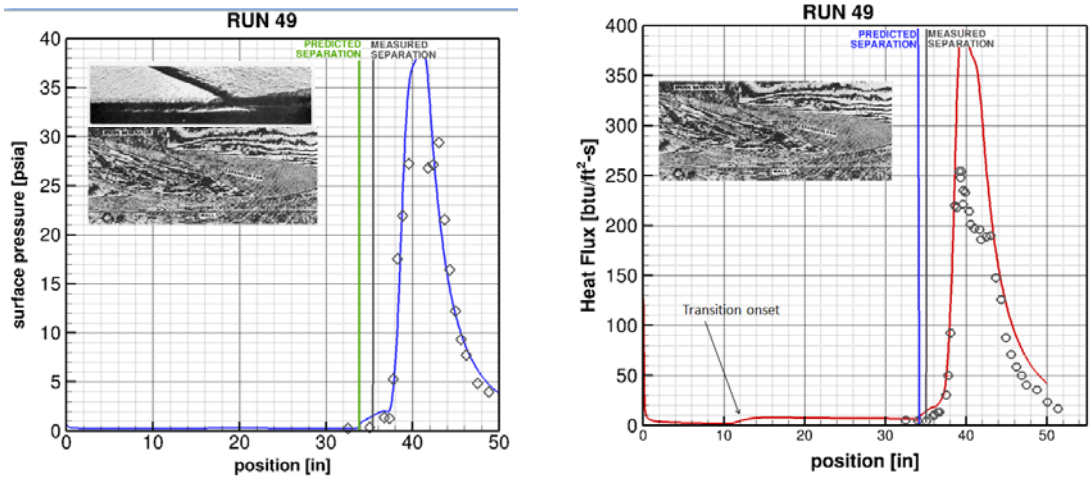

Figure 9 **Comparison between DPLR Navier/RANS Predictions and Measurements of Pressure and Heat Transfer in Separated Flow Induced by an Externally Generated Incident Shock on a Flat Plate**

Next, we show comparisons between the DPLR calculations, employing the turbulence models that were used "successfully" to predict the HIFiRE test cases, with measurements on a 9-ft long cone/flare configuration constructed many years ago over which the boundary layer is fully turbulent over 90 percent of the model length. Comparisons between the RANS predictions with the SA model and Wilcox stress limiter and experiment, shown in Figure 10, indicate that the separated region was significantly overpredicted, although the levels of pressure and heating upstream and downstream of the interaction region are relatively accurately predicted.

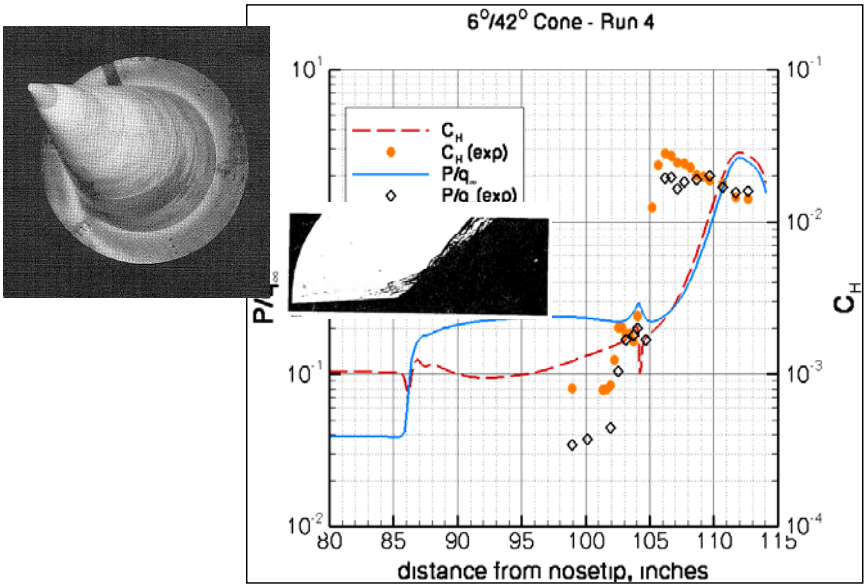

Figure 10 Comparison between DPLR Calculations and Measurements of the Pressure and Heat Transfer Distribution at the Cone/Flare Junction on the Large Cone Model

Diagrams of the models and instrumentation and tabulations of the measurements made for these test cases are presented in **Appendices A.1-A-4**

MEASUREMENTS FOR "BLIND" CODE VALIDATION STUDIES IN REGIONS OF SHOCK WAVE/TURBULENT BOUNDARY LAYER INTERACTION ON NEW CONE/FLARE AND HOLLOW CYLINDER/FLARE CONFIGURATION AT MACH NUMBERS FROM 6 TO 9 AT FLIGHT MATCHED ENTHALPIES

INTRODUCTION

We have performed experiments with a large double cone and hollow cylinder/flare model to examine regions of shock wave/turbulent boundary layer interaction for a range of high Reynolds number flow conditions from Mach 5 to 8. We will use these as a basis of "blind" validation exercise where we will provide only details of the model geometries and the test conditions at which these models were conducted. The models were instrumented to provide highly detailed surface pressure and heat transfer measurements both upstream and downstream, as well as in the interaction regions at the base of the flares. A key feature of these boundary layer studies is that the models employed in this program are very large so that transition occurs well upstream of the interaction region, and thus the influence of transition on the unsteady characteristics of the interaction region and the requirement to accurately predict the characteristics of the transition zone were minimized. However, we have also obtained detailed measurements in the transition regions to evaluate the performance of the prediction methods in these regions.

EXPERIMENTAL FACILITIES

The experimental studies reported here have been conducted in the CUBRC reflected shock tunnels. A summary of the performance of CUBRC's three major ground test facilities, the LENS I and II shock tunnels, and LENS XX expansion tunnel are listed in Figure 11. Velocity/altitude performance of the three LENS facilities is presented in Figure 12 and the Mach Number/Reynolds Number Capabilities for LENS I and II are shown in Figure 13. The LENS II tunnel, which has been employed in most of the studies of shock wave/turbulent boundary layer interaction, is operated principally to examine flows at Mach numbers between 3.5 and 10, and it is capable of fully duplicating test conditions on vehicles up to 30 ft in length. In

this tunnel, we also employ electrically heated models to bring the surface temperature of the vehicle to flight values. The LENS I facility overlaps with LENS II between Mach 8 and 10 and can be used to duplicate velocities up to 15,000 ft/s and Mach numbers up to 22.

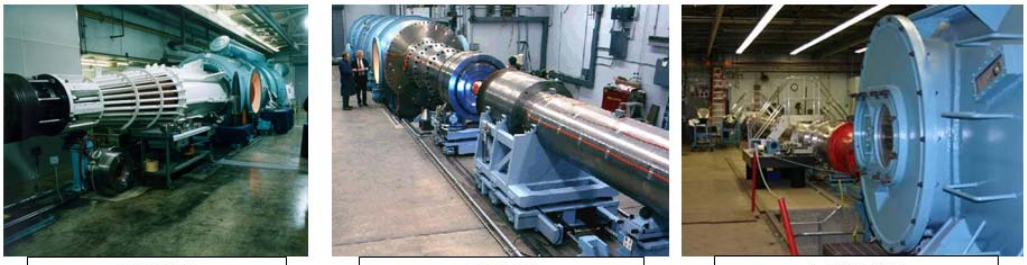

LENS I	LENS II	LENS XX
Velocity Range (ft/sec)	Velocity Range (ft/sec)	Velocity Range (ft/sec)
3,000 – 15,000	2,500 – 10,000	8,000 – 40,000
Altitude (kft)	Altitude (kft)	Altitude (kft)
25 – 300	SL - 200	SL - 250
Mach Numbers	Mach Numbers	Mach Numbers
7 – 16 (true duplication)	3 – 10	8 – 25
16 – 24 (Re-M only)	Reynolds Numbers (1/ft)	Reynolds Numbers (1/ft)
Reynolds Numbers (1/ft)	$10^5 – 10^9$	$10^3 – 10^9$
$10^4 – 10^8$	Test Time (ms)	Test Time
Test Time (ms)	up to 100 ms	up to 4 ms
up to 25 ms	Nozzles	Nozzles
Nozzles	Mach 3 – 5 (42" Exit)	Contoured for Mach
Mach 7 – 9 (44" Exit)	Mach 5 – 7 (60" Exit)	Numbers from 8 to 25
Mach 9 – 16 (44" Exit)	Mach 7 – 10 (72" Exit)	
Mach 15 – 24 (72" Exit)		

Figure 11 CUBRC Test Facilities to Investigate Shock Wave/Turbulent Boundary Layer Interaction Phenomena in Supersonic and Hypervelocity Flows

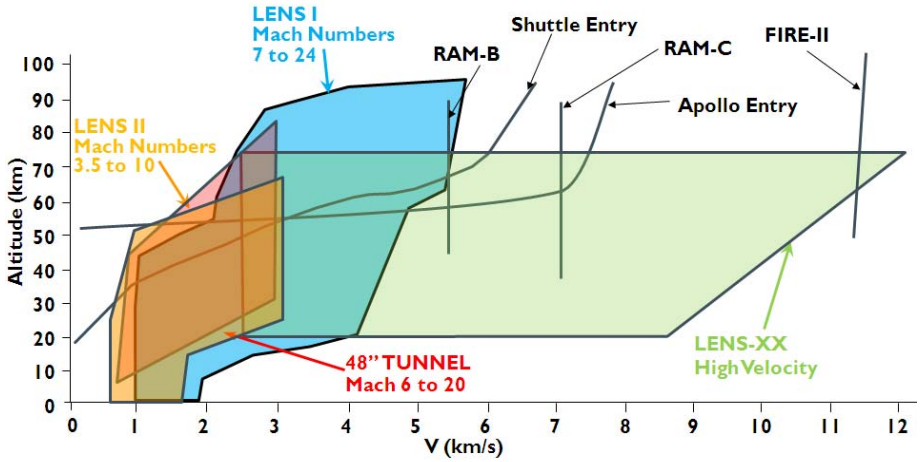

Figure 12 LENS Facilities Altitude/Velocity Map

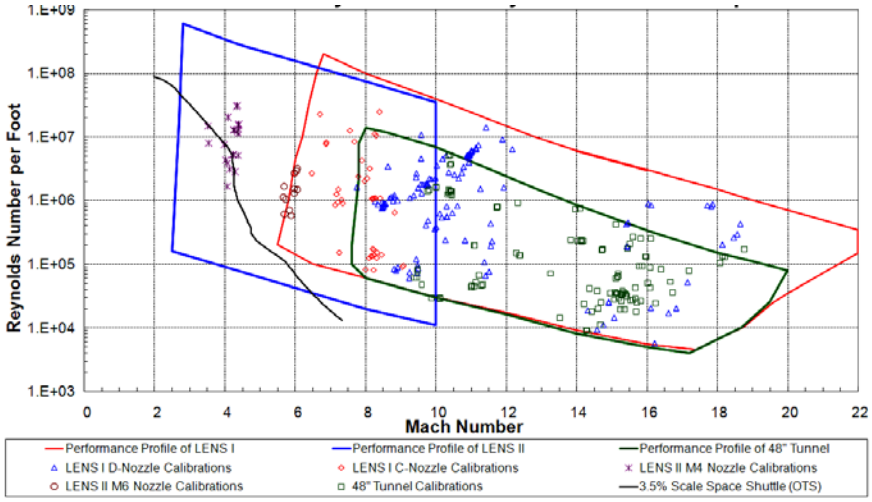

Figure 13 Mach Number/Reynolds Number Envelope for LENS Tunnels

The experimental studies conducted in the LENS II tunnel were conducted at freestream Mach numbers between 4 and 9 and Reynolds numbers up to 0.5 billion. They were also conducted for both "cold flow" and at flight enthalpies at each Mach number. The large scales of the models which are employed in these studies, coupled with the ability to generate Reynolds numbers up to 80 x 10^6 per foot, enables us to obtain transition within several inches of the leading edge of the models, thereby eliminating any questions as to the unsteady effects of transition on the mean and fluctuating characteristics of the interaction regions. In turn, the specific models employed to describe the transition regions in the CFD codes also must have little effect on the predictions of the characteristics of the shock interaction regions. During these studies, we have employed both intrusive and nonintrusive measurements to define the mean and fluctuating characteristics of the freestream. Using this information, we are evaluating the methods to predict transition onset (i.e., STABL[4], the CRAFT ETM[5], and semi-empirical design methods) in our ground test environment with the objective of developing rational methods to link ground test measurements to flight.

Evaluation of Test Conditions

The facility test conditions are established and validated by a combination of measurements in the reservoir region and test section of the tunnel. The stagnation pressure and enthalpy are obtained directly from pressure measurements behind the reflected shock and measurements of the incident shock Mach number. Conditions in the freestream are obtained from survey rakes containing pitot pressure probes, stagnation heat transfer gauges on hemispherical cylinders, total temperature measurements with vented thermocouple probes (where applicable), and cone pressure measurements to establish, in conjunction with the aforementioned measurements, the static pressure in the flow. Facility calibration is always supported by comparisons to numerical predictions. Calculations of the nozzle flowfield at each select test conditions have been performed using a specialized form of the DPLR code[6]. It employs the Spalart-Allmaras 1-equation turbulence model (Spalart and Allmaras[7]) with the Catris and Aupoix[8] compressibility correction. Non-ideal gas effects are included in the calculation because of the large pressures in the reservoir.[9] From these measurements and calculations, we can determine the accuracy of the freestream dynamic pressure and the stagnation point enthalpy to ± 5% and the Mach number to ±1.5%.

MODELS AND INSTRUMENTATION

Data sets for the "blind" validation studies were obtained with high-frequency surface pressure and heat transfer instrumentation installed in the new large cone/flare model and the large hollow cylinder/flare model shown installed in the 72-inch nozzle in the schematic diagrams in Figure 14. The double cone model was tested first in the LENS II tunnel in our Mach 4.5-to-6 nozzle with a 60-inch exit plane diameter as shown in Figure 15. The dimensions of this model are presented in Figure 16. The model is instrumented along its length with high-frequency thin-film heat transfer and piezoresistive pressure sensors, and as

shown in Figure 17, there is a high density of instrumentation at the cone/flare junction. In addition to Schlieren photography, flow field measurements were made with differential interferometry.

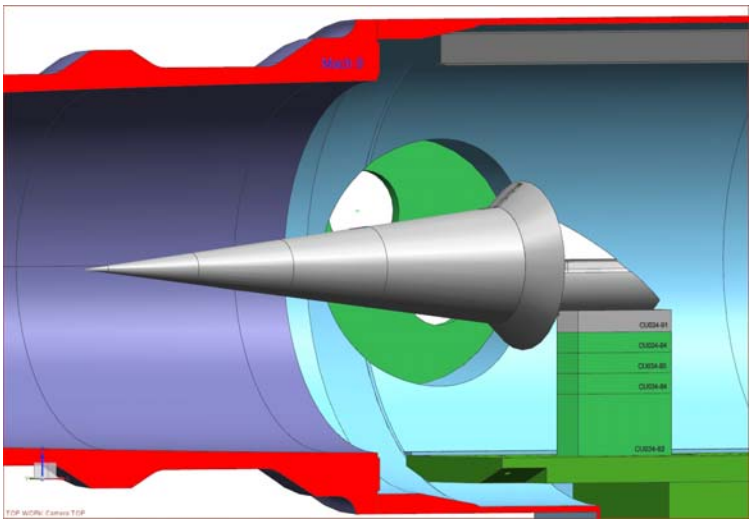

Figure 14 Large Hollow Cylinder/ Flare and Cone/Flare Model installed in the 72inch Mach 5 to 10 Contoured Nozzle

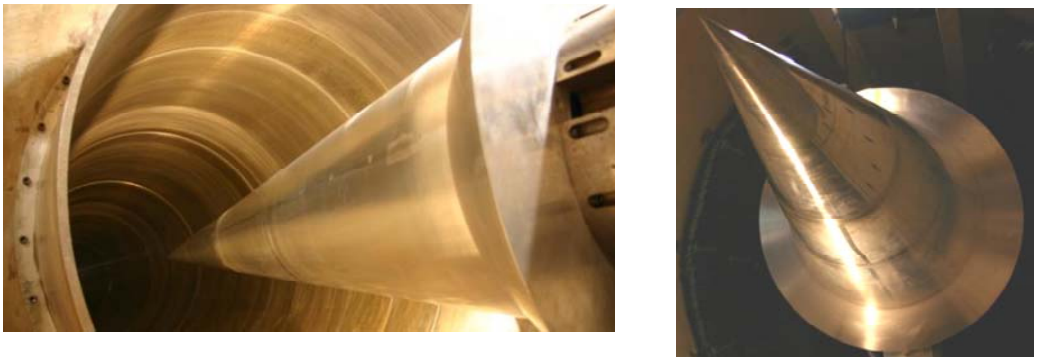

Figure 15 New Large Cone/Flare Model Constructed and Employed in the LENS II Tunnel at Mach 6 to 8 to Generate New Datasets for Blind Code Validation Studies

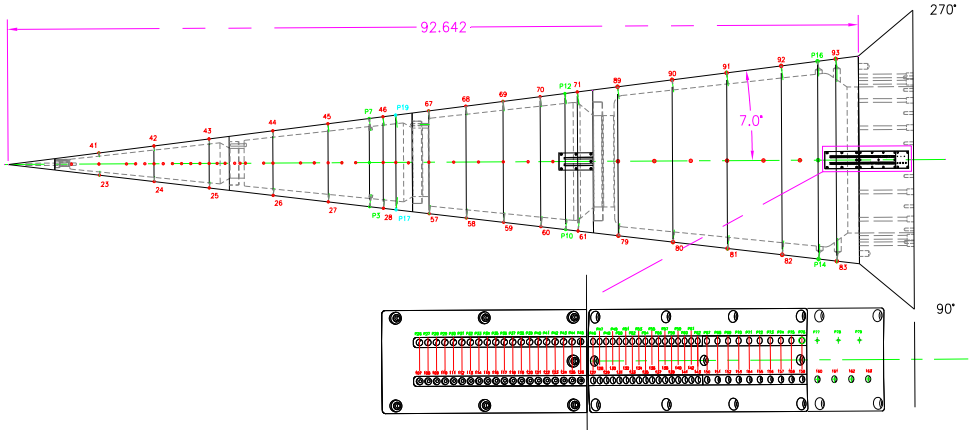

Figure 16 Model Dimensions and Instrumentation Layout of the New Large Cone/Flare Model

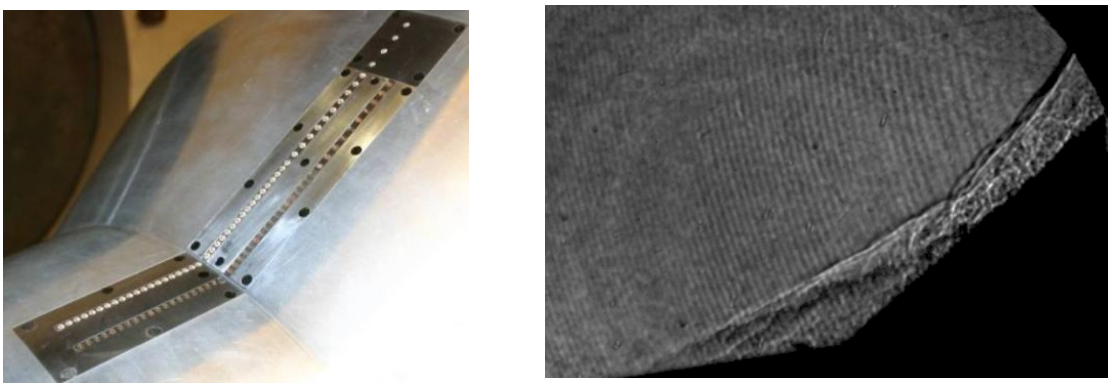

Figure 17 Instrumentation at Cone/Flare Junction on Large Cone Model and Schlieren Photograph of Transitional Flow over the Cone/Flare Junction (Not a new Test Case)

The dimensions of the new hollow cylinder/flare model are shown in Figure 18. This model is also highly instrumented at the cylinder/flare junction to provide detailed surface measurements on the size and turbulence properties throughout the interaction region as well as the attached turbulent flows both ahead and downstream of the separated interaction region This model is shown installed in the exit plane of the new Mach 7 to 10 nozzle in Figure 19. A photograph of the large hollow cylinder/flare model is shown in Figure 20 prior to installation in the LENS II tunnel.

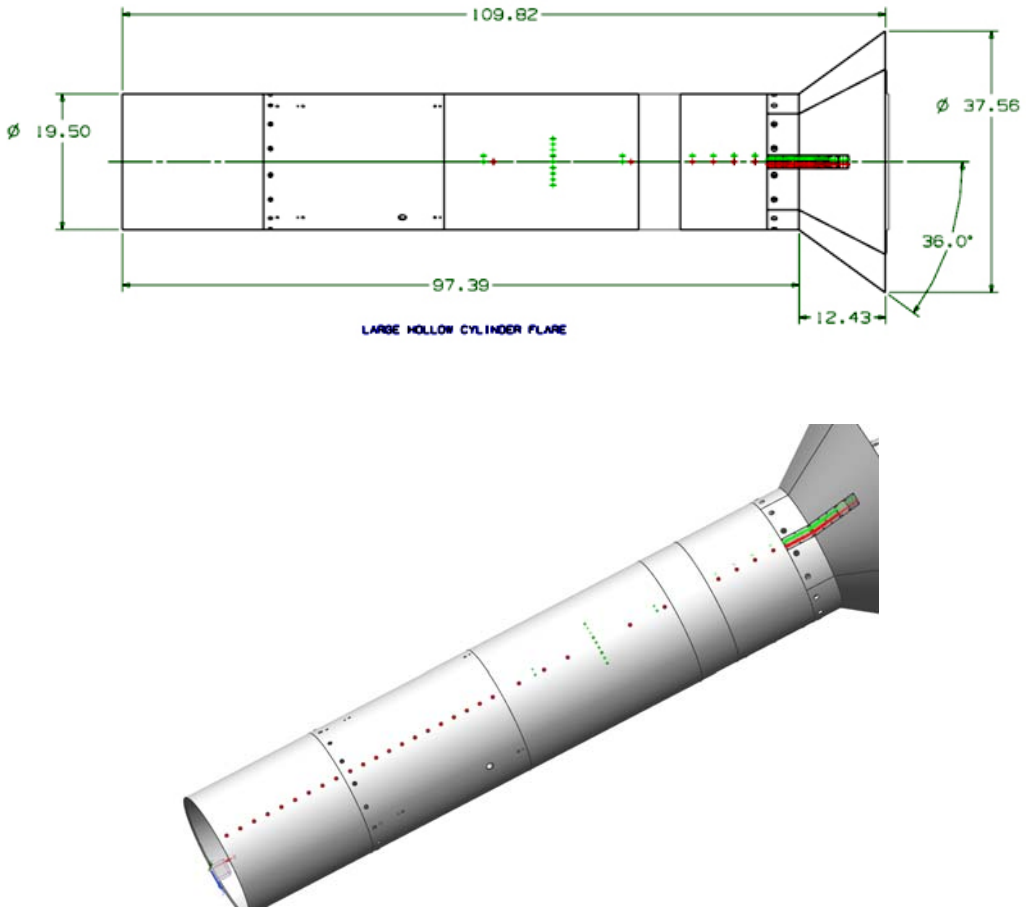

Figure 18 Model Dimensions and Instrumentation Layout of the Large Hollow Cylinder/Flare Model

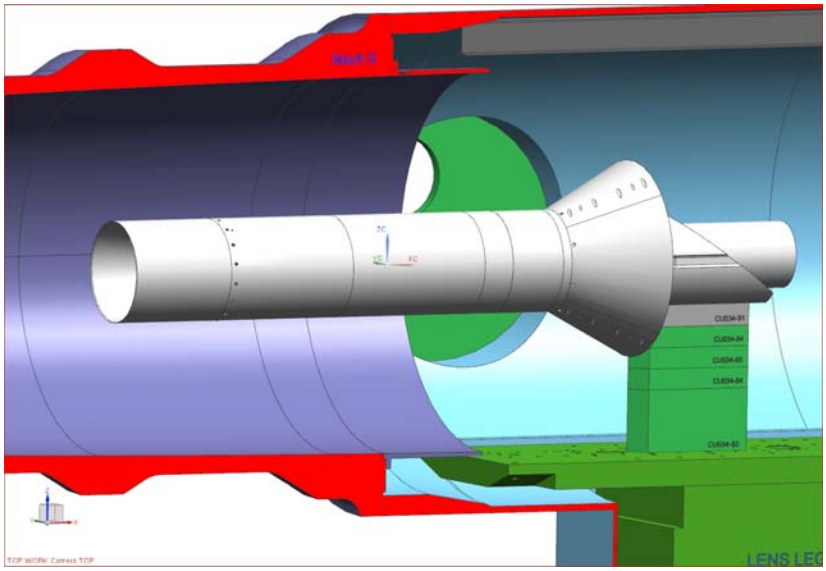

Figure 19 Large Hollow Cylinder Flare Installed in the LENS II 72-inch Contoured Mach 5 to 10 Nozzle

Figure 20 Photograph of Large Hollow Cylinder Flare Model

NEW DATASETS FOR CODE VALIDATION

Datasets have been collected from measurements made with both the large cone/flare model and hollow cylinder/flare model from tests conducted in the LENS facility at Mach numbers from 6, 7 and 8 at a number of high Reynolds number test conditions. Table I shows a typical set of basic freestream

conditions employed in the Mach 6 studies. Here it can be seen that measurements were obtained for both cold flow conditions and for true temperature flight conditions. Similar sets of measurements are being obtained on both the cone/flare and hollow cylinder/flare models at Mach numbers of 7 and 8. Again, at cold flow conditions and for conditions where we matched total enthalpy at the specific Mach number tested.

Run Number	Mach Number	Velocity	Temperature	Pressure	Density	Reynolds Number (Cone Length)	Tw/To
	-	(ft/sec)	(deg R)	(psia)	(slugs/ft^3)	(ReL)	-
1	6.04	3138.90	112.16	0.25	1.85E-04	5.15E+07	0.57
4	5.87	3249.50	127.04	0.12	7.66E-05	1.92E+07	0.53
5	6.00	5467.70	344.82	0.54	1.27E-04	2.05E+07	0.20
9	7.15	3485.03	98.89	0.05	4.00E-05	1.44E+07	0.48
10	7.01	6277.46	333.80	0.34	8.67E-05	1.62E+07	0.15
11	7.13	3440.73	96.93	0.32	2.73E-04	9.89E+07	0.49
12	7.00	6483.02	357.04	0.17	4.05E-05	7.35E+06	0.14
14	7.14	3380.71	93.32	0.16	1.42E-04	5.28E+07	0.52
17	7.16	3381.55	92.85	0.02	2.10E-05	7.86E+06	0.62
18	7.11	3457.93	98.46	0.32	2.76E-04	9.87E+07	0.49

Table 1 **Freestream Condition for Existing Large Cone Flare Validation Cases at Mach Numbers of 6 and 7**

Shown in Figure 21 are heat transfer measurements made during the experimental program of the heating rate along the cone demonstrating that transition occurs well ahead of the interaction region resulting in a well-defined turbulent boundary layer upstream of the cone/flare junction.

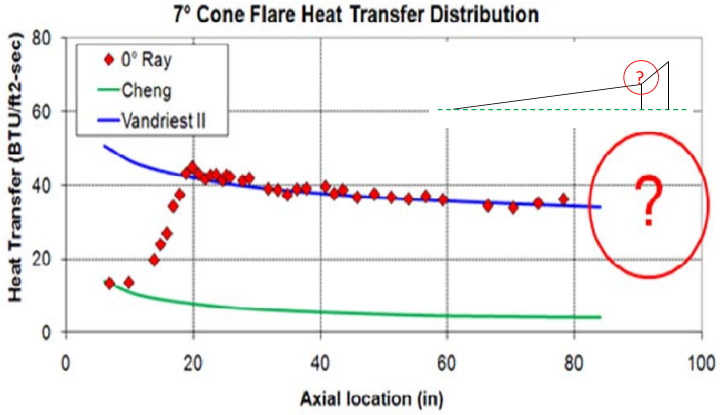

Figure 21 **Heat Transfer Measurements along the Cone Section of the Cone/Flare Model demonstrating the Fully Turbulent Nature of the Flow ahead of the Cone/Flare Junction**

Ideally, the computations to describe the shock interaction region should be initiated at the leading edge of both the hollow cylinder/flare and double cone model. The calculations should describe accurately the laminar boundary layer downstream of the leading edge, the transition region from laminar to turbulent flow, and the region of shock wave/turbulent boundary layer interaction. An important boundary condition for these calculations is the position of boundary layer transition. So to specify this point for each of the test cases, we have shown the laminar heating distribution on each model up to the point where the heat transfer rate indicates boundary layer transition has occurred. Shown in Figure 22 are typical measurements taken

on the forecone of the cone/flare model defining the laminar heating levels and the position at which the heating levels show that boundary layer transition is occurring.

Run Number	Laminar Heating Value at Transition Location	Location of Start of Transition	Location of Completion of Transition
	(Btu/ft^2-sec)	(inches)	(inches)
1.00	0.71	6.85	13.89
4.00	0.28	15.89	25.26
5.00	6.51	9.95	16.89
9.00	0.27	18.89	28.84
10.00	6.42	17.89	28.84
11.00	Turbulent Forward of First Sensor		
12.00	3.34	27.83	45.82
14.00	7.18	15.89	28.84
17.00	3.42	48.52	74.33
18.00	Turbulent Forward of First Sensor		

Figure 22 Laminar Heating Levels and Transition Locations for Double Cone Studies with Turbulent Heating

As discussed earlier, all the measurements for the "blind" code validation studies are being obtained at freestream conditions where boundary layer transition occurs well upstream of the interaction regions at conditions similar to those where the heat transfer measurements shown in Figure 21 were made. However, in companion studies where we were specifically looking at the characteristics of the transition process, measurements were made at lower Reynolds numbers and for these conditions the separated flow over the cone/flare junction was transitional in nature. A Schlieren photograph of this transitional flow is shown in Figure 23 and clearly this is not one of the test cases for the "blind" validation studies; however, we have shown the measured pressure distribution through this region in Figure 24 as an example of the detailed measurements made through the interaction region in the subsequent measurements at significantly larger Reynolds numbers.

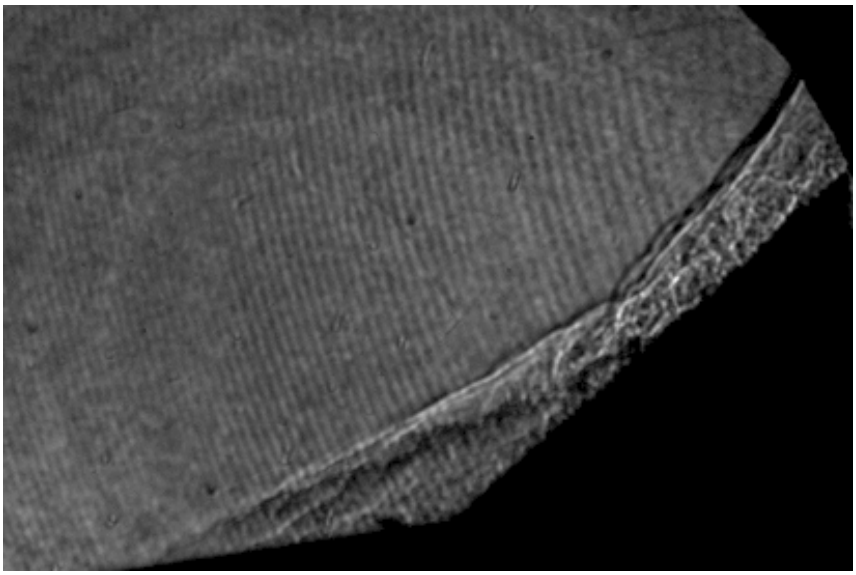

Figure 23 **Transitional Flow over Cone/Flare Model at Much Lower Reynolds Numbers than used for the Fully Turbulent Interaction Studies**

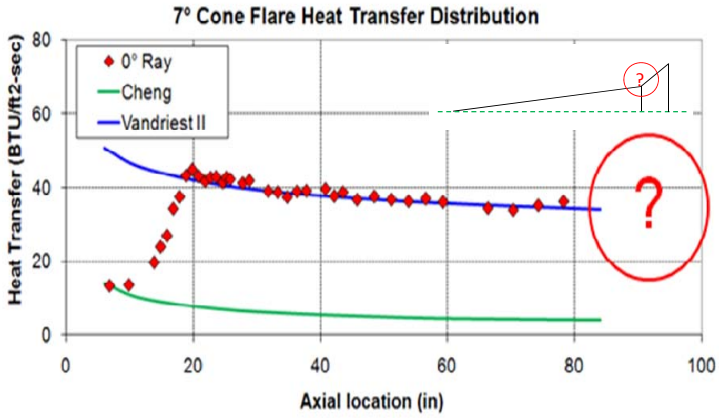

(TIM REPLACE THIS)

Figure 24 Distribution of Pressure for Transitional Interaction

SUMMARY AND CONCLUSIONS

Experimental studies have been conducted to examine the characteristics of regions of shock wave/turbulent boundary layer interaction over cone/flare and hollow cylinder/flare configurations in high Reynolds number flows at Mach numbers from 5 to 10 in cold flows and at duplicated flight velocities. Detailed surface pressure and heat transfer measurements have been made through the separated interaction regions as well as upstream and downstream of the interactions for a range of Reynolds numbers under cold wall conditions for total enthalpies matching flight, as well as at lower enthalpies which matched measurements made earlier for low temperature freestream conditions. The large scale of the models used in these experiments enabled us to obtain measurements in fully turbulent flows with the length of turbulent flow up to 1,000 boundary layer thicknesses downstream of the beginning of untripped transition. The surface measurements obtained in these studies together with Schlieren and interferometry measurements of the regions of shock wave/boundary layer interaction have been assembled to provide data sets for "blind" code validation studies. We have also included detailed information on the results of experimental

studies of shock wave/boundary layer interaction conducted earlier which can also be used to evaluate the models of turbulence employed in CFD codes.

ACKNOWLEDGEMENT

The work presented in this paper was performed with funding from AFOSR Grant No. FA9550-11-1-0290.

References:

1. Holden, Michael S. and Wadhams, Timothy, P., "Code Validation Study of Laminar Shock/Boundary Layer and Shock/Shock Interactions in Hypersonic Flow Part A: Experimental Measurements," AIAA 2001-1031, 39th AIAA Aerospace Sciences Meeting and Exhibit, Reno, NV, January 8-12, 2001. Harvey, John K., Holden, Michael S., and Wadhams, Timothy P., "Code Validation Study of Laminar Shock/Boundary Layer and Shock/Shock Interactions in Hypersonic Flow. Part B: Comparisons with Navier-Stokes and DSMC Solutions," AIAA 2001-1031, 39th AIAA Aerospace Sciences Meeting and Exhibit, Reno, NV, January 8-12, 2001.

2. Wadhams, T., Mundy, E., MacLean, M., and Holden, M., "Ground Test Studies of the HIFiRE-1 Transition Experiment Part 1: Experimental Results," *Journal of Spacecraft and Rockets.* Vol. 45, No. 6, pp 1134-1148. Nov-Dec 2008.

3. MacLean, M., Wadhams, T., Holden, M., and Johnson, H., "Ground Test Studies of the H IFiRE-1 Transition Experiment Part 2: Computational Analysis," *Journal of Spacecraft and Rockets.* Vol. 45, No. 6, pp 1149-1164. Nov-Dec. 2008

4. Johnson, H., and Candler, G., "Hypersonic Boundary Layer Stability Analysis using PSE-Chem.", AIAA Paper 3005-5023, 35th AIAA Fluid Dynamics Conference and Exhibit, Toronto, ON, June 2005.

5. Papp, J.L., Kenzakowski, D.C., and Dash, S.M., "Extensions of a Rapid Engineering Approach to Modeling Hypersonic Laminar to Turbulent Transitional Flows," AIAA Paper 2005-0892, 43rd Aerospace Sciences Meeting & Exhibit, Reno, NV; 10-13 January 2005.

6. Candler, Graham V. "Hypersonic Nozzle Analysis Using an Excluded Volume Equation of State". AIAA Paper 2005–5202. 38TH AIAA Thermophysics Conference, Toronto, CA: 6 – 9 June 2005.

7. Spalart, P.R. and Allmaras S.R. "A One-Equation Turbulence Model for Aerodynamic Flows". AIAA Paper 92-0439. 30TH Aerospace Sciences Meeting & Exhibit. Reno, NV: 6-9 Jan, 1992.

8. Catris S. and Aupoix B. "Improved Turbulence Models for Compressible Boundary Layers." AIAA Paper 98-2696. 2ND Theoretical Fluid Mechanics Meeting: Albuquerque, NM, June 1998.

9. MacLean, M.; Candler, G.; and Holden, M. "Numerical Evaluation of Flow Conditions in the LENS Reflected Shock-Tunnel Facilities". AIAA Paper 2005-0903. 43rd Aerospace Sciences Meeting & Exhibit. Reno, NV: 10-14 January 2005.

10. Lordi, J.A. and Mates, R.E., "Non-equilibrium Expansions of High-Enthalpy Airflows," Cornell Aeronautical Laboratory Report, ARL64-206, November 1964.

11. Menter, F.R. "Two-Equation Eddy-Viscosity Turbulence Models for Engineering Applications". *AIAA Journal*. Vol. 32, No. 8, pp 1598 – 1605. August 1994.

12. Wilcox, David C. *Turbulence Modeling for CFD*. 3RD Ed. La Canada, CA: DCW Industries, Inc, November 2006.

Appendix A.

A.1 Flat Plate/ Wedge Data and Conditions for Run 54

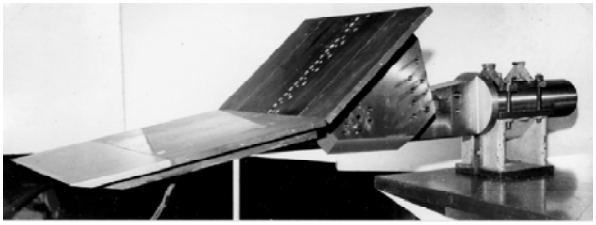

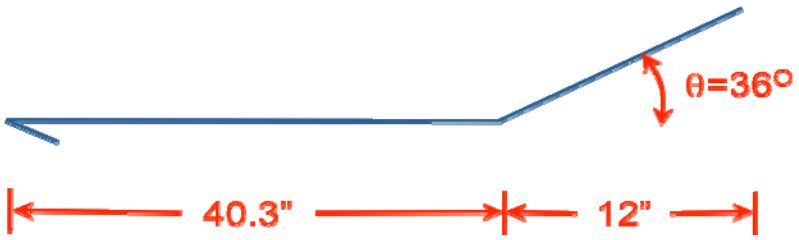

ρ, sl/ft^3	T, R	U, ft/s	M
1.600x10^{-4}	110	5,802	11.3

X, in	qw, btu/ft^2-s	X,in	p, psia	X,in	tau, psia
32.52	4.39	32.53	0.206	32.53	0.00615
34.02	4.82	35.02	0.221	36.72	0.00868
35.04	4.5	36.72	0.204	37.21	0.01
35.93	4	37.31	0.198	37.75	0.00204
36.13	4.13	37.75	0.327	38.27	-0.00299
36.48	4.19	38.27	0.76	39.56	-0.0055
36.69	4.1	38.82	1.15	40.48	0.0114
37.56	4	39.56	1.08	42.39	0.571
37.76	3.98	41.78	10.2	43.32	0.4
38.08	9.5	42.38	16.5	45.27	0.245
38.61	8.85	43.02	16.6	47.19	0.247
38.82	10.5	43.67	14.3		
39.13	10.4	44.31	14.9		
39.28	9.81	44.94	15.4		
39.42	10.2	45.59	14.9		
39.59	9.91	46.22	14.6		
39.68	10.9	47.5 14.5			

39.89	12	48.79	16.5		
40.36	33.1	50.07	15		
40.56	56.5	51.36	14.4		
41.01	94.2				
41.21	107				
41.66	176				
41.85	210				
42.3	195				
42.5	181				
43.02	160				
43.67	146				
44.31	142				
44.94	125				
45.59	116				
46.22	107				
46.87	107				
47.5	99.9				
48.79	105				
50.07	97.7				
51.36	88.7				

X represents axial distance from the leading edge

A.2 Shock Generator/ Flat Plate . Data and Conditions for Run 49

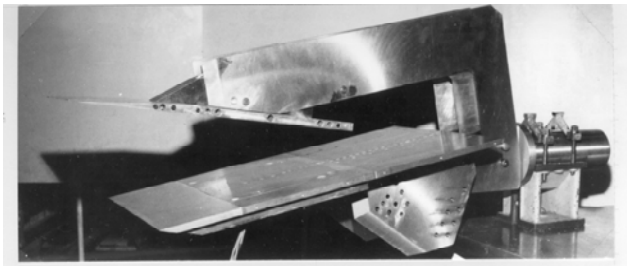

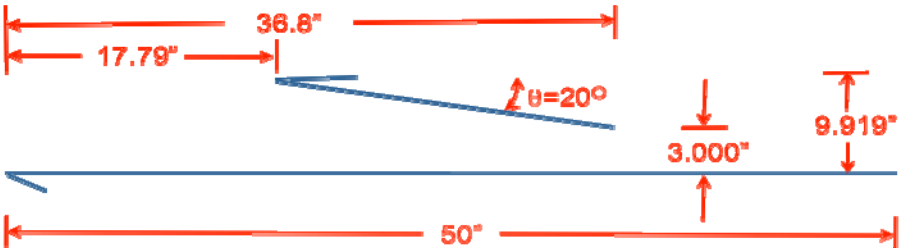

ρ, sl/ft^3	T, R	U, ft/s	M
1.729x10^{-4}	113	5,950	11.4

X, in	qw, btu/ft^2-s	X,in	p, psia	X,in	tau, psia
32.52	5.16	32.53	0.241	32.53	0.00662
34.02	5.04	35.02	0.323	36.72	-0.00562
35.04	4.25	36.72	1.35	37.21	-0.00481
35.93	10	37.31	1.25	37.75	-0.05
36.13	11.1	37.75	5.26	38.27	-0.0155
36.48	13.2	38.27	17.5	39.56	0.4
36.69	13.6	38.82	21.9	40.48	0.485
37.56	30.4	39.56	27.2	42.39	0.413
37.76	50	41.78	26.8	45.27	0.181
38.08	92.4	42.38	27.1	47.19	0.127
38.61	220	43.02	29.4		
38.82	218	43.67	21.5		
39.13	254	44.31	16.4		
39.28	248	44.94	12.2		
39.42	254	45.59	9.33		
39.59	221	46.22	7.72		
39.68	235	47.5 4.81			
39.89	233	48.79	3.96		

40.36	214	50.07	2.89	
40.56	201	51.36	1.87	
41.01	197			
41.66	196			
41.85	186			
42.5	189			
43.02	190			
43.67	148			
44.31	126			
44.94	87.8			
45.59	70.9			
46.22	58.7			
46.87	50.3			
47.5	40.6			
48.79	35.6			
50.07	23.6			
51.36	16.8			

X represents axial distance from the leading edge

A.3 Large Cone Flare Model Data and Conditions for Large Cone/Flare Run 4

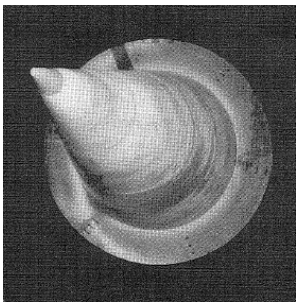

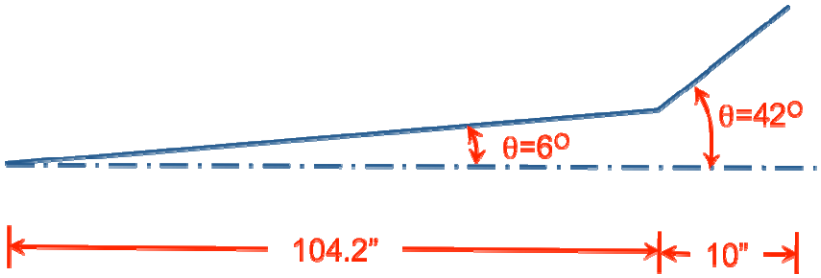

ρ, sl/ft^3	T, R	U, ft/s	M
6.345x10^{-5}	121	5,920	11.0

X, in	$C_H=q/[\rho U(h_0-h_W)]$	X,in	p/q_∞
98.91	0.000805	98.910	0.034617
101.32	0.000787	100.12	0.037367
101.61	0.000798	101.92	0.044641
101.92	0.000847	102.51	0.104292
102.22	0.001240	103.11	0.167478
102.51	0.002023	103.72	0.179795
102.81	0.002017	104.02	0.198549
103.11	0.001816	104.68	0.168566
103.42	0.001830	106.18	1.931486
103.72	0.001642	106.68	1.957518
104.02	0.002398	107.18	1.639943
105.18	0.012382	107.68	1.812071
105.68	0.023679	108.68	1.880974
106.18	0.027989	109.68	1.997410
106.68	0.027113	110.68	1.677503
107.18	0.024481	111.68	1.553167
107.68	0.024153	112.68	1.590079

108.18	0.022741	
108.68	0.020162	
109.18	0.019826	
109.68	0.018754	
110.68	0.017763	
111.68	0.014434	
112.68	0.014068	

X represents axial distance from the sharp nosetip

A.4 HIFiRE-1/2 Cone/Cylinder/Flare Run 30

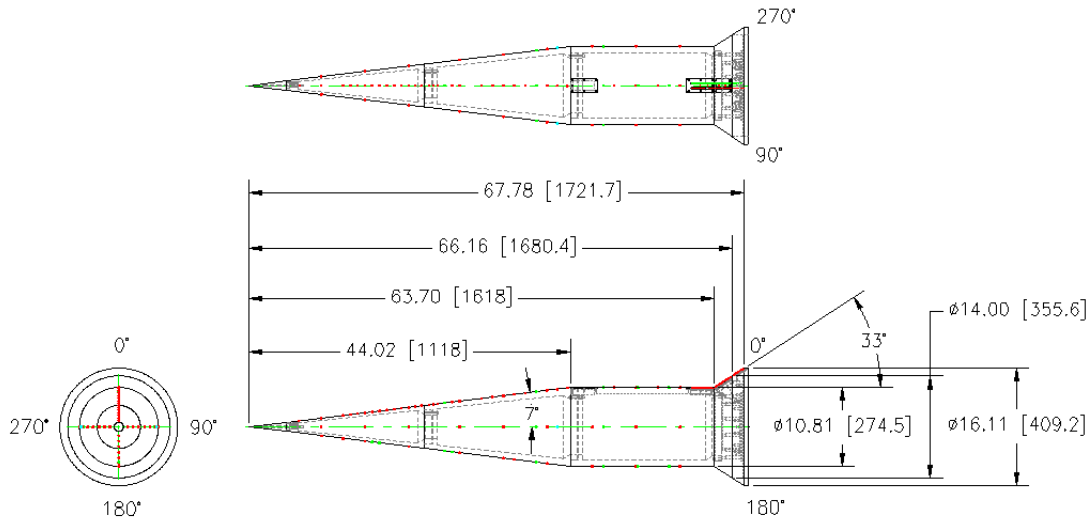

ρ, sl/ft^3	T, R	U, ft/s	M
1.3x10^{-4}	408	7,120	7.19

X, in	qw, btu/ft^2-s	X,in	p, psia
6.848	18.920	26.834	1.553
9.892	15.984	39.342	1.561
13.892	12.151	48.516	0.503
14.892	12.954	53.266	0.485
15.892	12.384	57.516	0.479
16.892	12.357	60.643	0.456
17.892	18.669	60.953	0.494
18.892	24.482	61.108	0.424
19.892	26.909	61.263	0.754
20.892	36.284	61.418	0.780
21.892	41.865	61.573	0.749
22.761	47.132	61.728	0.755

23.631	53.914
24.672	45.004
25.257	44.441
25.842	44.395
27.827	44.368
28.842	41.540
31.842	42.174
33.342	40.422
34.842	41.556
36.342	40.926
37.842	40.622
40.842	38.636
42.217	39.119
43.592	36.754
50.016	12.659
53.016	11.655
56.016	11.917
59.016	11.727
60.643	11.723
60.798	12.053
60.953	12.875
61.108	12.047
61.263	12.409
61.418	13.688
61.573	14.711
61.728	15.321
61.883	16.664
62.038	16.503
62.193	15.586
62.348	15.438
62.503	15.298
62.658	16.812
62.813	18.736
62.968	20.980
63.123	22.286
63.278	23.326
63.433	25.721
63.588	31.114
63.813	37.425
61.883	0.835
62.038	1.542
62.193	1.343
62.503	1.153
62.658	1.407
62.813	1.725
62.968	1.253
63.123	1.503
63.278	1.213
63.433	2.250
63.588	2.288
63.813	1.998
63.943	2.389
64.073	3.059
64.203	3.689
64.333	4.331
64.463	4.845
64.593	6.389
64.723	6.817
64.853	8.210
64.983	10.824
65.113	13.877
65.503	16.441
65.633	17.748
65.763	18.466
65.893	19.082
66.368	16.831
66.703	16.972
67.039	16.605
67.374	16.598

63.943	48.892	
64.073	59.491	
64.203	71.687	
64.333	85.973	
64.463	107.734	
64.593	118.448	
64.723	139.267	
64.853	156.220	
64.983	176.113	
65.113	205.019	
65.243	228.316	
65.373	239.008	
65.503	266.669	
65.633	293.006	
65.763	304.615	
65.893	273.236	
66.368	265.986	
66.535	255.345	
66.703	259.736	
66.871	255.090	
67.039	254.170	
67.206	247.960	
67.374	244.740	
67.542	249.010	
67.710	236.400	

X represents axial distance from the virtual sharp nose (2.5-mm nose radius for Run 30)